Viscosities of the Baryon-Rich Quark-Gluon Plasma from Beam Energy Scan Data

Chun Shen[1,2] Björn Schenke,[3] and Wenbin Zhao[1,4,5]

[1]*Department of Physics and Astronomy, Wayne State University, Detroit, Michigan 48201, USA*
[2]*RIKEN BNL Research Center, Brookhaven National Laboratory, Upton, New York 11973, USA*
[3]*Physics Department, Brookhaven National Laboratory, Upton, New York 11973, USA*
[4]*Nuclear Science Division, Lawrence Berkeley National Laboratory, Berkeley, California 94720, USA*
[5]*Physics Department, University of California, Berkeley, California 94720, USA*

This work presents the first Bayesian inference study of the $(3+1)$D dynamics of relativistic heavy-ion collisions and quark-gluon plasma viscosities using an event-by-event $(3+1)$D hydrodynamics + hadronic transport theoretical framework and data from the Relativistic Heavy Ion Collider Beam energy scan program. Robust constraints on initial state nuclear stopping and the baryon chemical potential-dependent shear viscosity of the produced quantum chromodynamic (QCD) matter are obtained. The specific bulk viscosity of the QCD matter is found to exhibit a preferred maximum around $\sqrt{s_{NN}} = 19.6$ GeV. This result allows for the alternative interpretation of a reduction (and/or increase) of the speed of sound relative to that of the employed lattice-QCD based equation of state for net baryon chemical potential $\mu_B \sim 0.2(0.4)$ GeV.

Introduction.—The characterization of quark-gluon plasma (QGP) has long been a central pursuit in high-energy nuclear physics [1,2]. The Relativistic Heavy Ion Collider (RHIC) at Brookhaven National Laboratory has played a pivotal role in this endeavor, providing opportunities for studying strongly interacting matter at extreme temperatures and densities. One of the most intriguing aspects of RHIC experiments is the beam energy scan (BES) program [3–6], which systematically varies the center-of-mass energy of colliding ions to investigate the properties of the QGP over a wide range of the temperature and baryon chemical potential dependent phase diagram of quantum chromodynamics (QCD). The BES program allows us to investigate the transition between hadronic matter and the QGP and to search for a possible critical point and first-order phase boundaries, shedding light on the emergent properties of the nuclear force (see reviews [7–10]).

The theoretical description of the QGP and its real-time evolution in relativistic heavy-ion collisions is a complex and multifaceted challenge [11–15]. While relativistic viscous hydrodynamics is an efficient and effective framework to describe the QGP collectivity, uncertainties in the initial conditions and the transport properties of the medium introduce significant ambiguities in the theoretical predictions. Quantifying these uncertainties is essential for extracting precise information about the QGP's properties [16–22].

While it is challenging to compute the QGP transport coefficients from first principles (see [23] for recent lattice extractions of viscosities for a purely gluonic system), phenomenological studies showed that hadronic observables measured in heavy-ion collisions are sensitive to the shear and bulk viscosity of QCD matter [13,16,24–28]. Early work constraining these transport coefficients with hydrodynamic simulations of heavy-ion collisions generally focused on the shear viscosity, approximated as an effective constant ratio to the entropy density η/s [16,25,29,30]. Contemporary efforts adopted the Bayesian inference method to constrain the QGP's specific shear and bulk viscosities, including the uncertainties from all the other model parameters. Large-scale model-to-data comparisons are necessary to achieve this goal, given the significant computational challenge of constraining a high-dimensional model parameter space [31–42].

Aiming to make extensive use of existing rapidity and collision energy dependent data, we perform comprehensive modeling of the $(3+1)$D QGP dynamics in a 26-dimensional model parameter space with state-of-the-art relativistic viscous hydrodynamics + hadronic transport simulations. This is a significant extension over an earlier work [33], which studied a much smaller five-dimensional model parameter space. By performing the Bayesian inference analysis with multisystem measurements from the RHIC BES program phase I, we will obtain robust constraints on initial-state nuclear stopping and the temperature and baryon chemical potential dependent QGP shear and bulk viscosities for the first time.

Hybrid framework and model parametrizations.—To model the dynamics of Au + Au collisions from $\sqrt{s_{NN}} = 7.7$ to 200 GeV in the RHIC BES program, we employ a $(3+1)$D dynamical initialization model (3D-Glauber) coupled with the hybrid framework of relativistic viscous hydrodynamics (MUSIC) + hadronic transport (URQMD) [43,44]. The 3D-Glauber model simulates the initial stage

of heavy-ion collisions as the two nuclei pass through each other. Individual nucleon-nucleon (NN) collisions are determined based on their transverse positions and the inelastic NN cross section at the given collision energy. For each NN collision, we select valence quarks and soft partons inside the colliding nucleons to lose energy [44]. To constrain the initial-state nuclear stopping in this analysis, we parametrize the average amount of rapidity loss for each parton pair as a piecewise function,

$$
\langle y_{\text{loss}} \rangle =
\begin{cases}
y_{\text{loss},2} \frac{y_{\text{init}}}{2} & 0 < y_{\text{init}} \leq 2 \\
y_{\text{loss},2} + (y_{\text{loss},4} - y_{\text{loss},2}) \frac{y_{\text{init}}-2}{2} & 2 < y_{\text{init}} < 4 , \\
y_{\text{loss},4} + (y_{\text{loss},6} - y_{\text{loss},4}) \frac{y_{\text{init}}-4}{2} & y_{\text{init}} \geq 4
\end{cases}
$$

where the parameter $y_{\text{loss},n}$ specifies the average amount of rapidity loss for $y_{\text{init}} = n$. The event-by-event fluctuations of rapidity loss are introduced by the variance parameter $\sigma_{y_{\text{loss}}}$ [44]. After individual NN collision, wounded partons are decelerated with a string tension in the longitudinal direction during the time $\tau_{\text{hydro}} = 0.5$ fm/c in the collision rest frame. The lost energy and momentum produce an energy-momentum current J^μ, which is fed into the hydrodynamic fields via a source term,

$$
\partial_\mu T^{\mu\nu} = J^\mu, \qquad \partial_\mu J_B^\mu = \rho_B. \tag{1}
$$

In the second equation, baryon charge densities from incoming nucleons are treated as scalar sources to the hydrodynamic net baryon current [44].

We parametrize a blast-wave-like preequilibrium transverse flow profile for each string, developed during its hydrodynamization period τ_{hydro} with the transverse flow rapidity [45], $\eta_\perp(\mathbf{x}_\perp) = \alpha_{\text{preFlow}}|\tilde{\mathbf{x}}_\perp|$, where the 2D vector $\tilde{\mathbf{x}}_\perp = (x - x_{\text{string}}, y - y_{\text{string}})$, with x_{string} and y_{string} the coordinates of the string in the transverse plane, and the parameter α_{preFlow} controls the size of the preequilibrium flow. Then, the energy-momentum current J^μ can be written as

$$
J^\mu(\mathbf{x}_\perp, \eta_s) = e_{\text{string}}(\mathbf{x}_\perp, \eta_s) u_{\text{string}}^\mu[\eta_\perp(\mathbf{x}_\perp), y(\eta_s)], \tag{2}
$$

where the string's local flow velocity is $u_{\text{string}}^\mu(\eta_\perp, y) = (\cosh\eta_\perp \cosh y, \sinh\eta_\perp \hat{\mathbf{e}}_{\tilde{\mathbf{x}}_\perp}, \cosh\eta_\perp \sinh y)$ with $\hat{\mathbf{e}}_{\tilde{\mathbf{x}}_\perp} = \tilde{\mathbf{x}}_\perp/|\tilde{\mathbf{x}}_\perp|$ being the unit vector of $\tilde{\mathbf{x}}_\perp$ in the transverse plane. The transverse shape of the source terms $e_{\text{string}}(\mathbf{x}_\perp, \eta_s)$ is parametrized as Gaussian profiles with width σ_x^{string}. Precise definitions of $e_{\text{string}}(\mathbf{x}_\perp, \eta_s)$ and $y(\eta_s)$ can be found in Ref. [44]. The hydrodynamic equations of motion are solved with a lattice-QCD-based equation of state (EOS) at finite densities, NEOS-BQS, which imposes strangeness neutrality and $n_Q = 0.4 n_B$ for Au + Au collisions [46].

To account for shear and bulk viscous effects in the hydrodynamic phase [47–49], we parametrize the baryon chemical potential μ_B dependence of the QGP shear viscosity as

$$
\tilde{\eta}(\mu_B) =
\begin{cases}
\eta_0 + (\eta_2 - \eta_0)\frac{\mu_B}{0.2} & 0 < \mu_B \leq 0.2 \text{ GeV} \\
\eta_2 + (\eta_4 - \eta_2)\frac{(\mu_B - 0.2)}{0.2} & 0.2 < \mu_B < 0.4 \text{ GeV}, \\
\eta_4 & \mu_B \geq 0.4 \text{ GeV}
\end{cases} \tag{3}
$$

where $\tilde{\eta} \equiv \eta T/(e + P)$ and the parameters η_0, η_2, η_4 are the values of the QGP specific shear viscosity at $\mu_B = 0$, 0.2, 0.4 GeV, respectively. The translation from $\tilde{\eta}$ to η/s introduces a mild temperature dependence at finite net baryon density, namely, $\eta/s(T, \mu_B) = [1 + (\mu_B n_B/Ts)]\tilde{\eta}(\mu_B)$. To limit the number of model parameters, we do not include an explicit temperature dependence for $\tilde{\eta}$ here, since the results from previous Bayesian analyses were compatible with a temperature independent η/s value in the phase described by hydrodynamics [37].

The specific bulk viscosity is parametrized as an asymmetric Gaussian in temperature [13,28],

$$
\tilde{\zeta}(T, \mu_B) =
\begin{cases}
\zeta_{\text{max}} \exp\left[-\frac{(T - T_\zeta(\mu_B))^2}{2\sigma_{\zeta,-}^2}\right] & T < T_\zeta(\mu_B) \\
\zeta_{\text{max}} \exp\left[-\frac{(T - T_\zeta(\mu_B))^2}{2\sigma_{\zeta,+}^2}\right] & T \geq T_\zeta(\mu_B)
\end{cases}, \tag{4}
$$

where $\tilde{\zeta} \equiv \zeta T/(e + P)$ and the bulk peak temperature $T_\zeta(\mu_B) = T_{\zeta,0} - (0.15/1 \text{ GeV})\mu_B^2$, so that it closely follows the constant energy density curve with $e = e(T_{\zeta,0}, \mu_B = 0)$ for the NEOS-BQS EOS [46]. This ensures that the bulk viscosity peak closely follows the phase crossover at finite net baryon density [10,50,51].

Below the switching energy density e_{sw}, individual fluid cells are converted into hadrons according to the Cooper-Frye particlization procedure, including out-of-equilibrium corrections to particle distributions with multiple conserved charge currents (B, Q, S) using the Grad moment method [45]. The produced hadrons are then fed to the URQMD transport model for hadronic scatterings and decays [52,53]. The hadronic transport model controls the nontrivial (T, μ_B) dependence of viscosity in the dilute hadronic phase [54], which we do not vary in this Bayesian analysis.

All model parameters are listed in Table I with their prior ranges. The definitions of the parameters B_G, $\alpha_{\text{shadowing}}$, λ_B, $\sigma_\eta^{\text{string}}$, $\alpha_{\text{string tilt}}$ can be found in Ref. [44].

To obtain an estimate of the μ_B dependence of the bulk viscosity, we allow the model parameters ζ_{max} and $\sigma_{\zeta,\pm}$ to be independent parameters at different collision energies. This approach yields an effective μ_B dependence of ζ/s, in line with the general RHIC beam energy scan approach to probe QCD matter properties at finite net baryon density [55]. This

TABLE I. The 20 model parameters and their prior ranges.

Parameter	Prior	Parameter	Prior
B_G (GeV^{-2})	[1, 25]	$\alpha_{\text{string tilt}}$	[0, 1]
$\alpha_{\text{shadowing}}$	[0, 1]	α_{preFlow}	[0, 2]
$y_{\text{loss,2}}$	[0, 2]	η_0	[0.001, 0.3]
$y_{\text{loss,4}}$	[1, 3]	η_2	[0.001, 0.3]
$y_{\text{loss,6}}$	[1, 4]	η_4	[0.001, 0.3]
$\sigma_{y_{\text{loss}}}$	[0.1, 0.8]	ζ_{max}	[0, 0.2]
α_{Rem}	[0, 1]	$T_{\zeta,0}$ (GeV)	[0.15, 0.25]
λ_B	[0, 1]	$\sigma_{\zeta,+}$ (GeV)	[0.01, 0.15]
σ_x^{string} (fm)	[0.1, 0.8]	$\sigma_{\zeta,-}$ (GeV)	[0.005, 0.1]
$\sigma_\eta^{\text{string}}$	[0.1, 1]	e_{sw} (GeV/fm^3)	[0.15, 0.5]

TABLE II. The experimental measurements in Au + Au collisions used in this Bayesian inference study.

$\sqrt{s_{\text{NN}}}$ (GeV)	STAR	PHOBOS
200	$dN/dy(\pi^+, K^+, p, \bar{p})$ [58] $\langle p_T \rangle(\pi^+, K^+, p, \bar{p})$ [58] $v_2^{\text{ch}}\{2\}$ [59], $v_3^{\text{ch}}\{2\}$ [60]	$dN^{\text{ch}}/d\eta$ [61] $v_2^{\text{ch}}(\eta)$ [62]
19.6	$dN/dy(\pi^+, K^+, p)$ [55] $\langle p_T \rangle(\pi^+, K^+, p, \bar{p})$ [55] $v_2^{\text{ch}}\{2\}$ [59], $v_3^{\text{ch}}\{2\}$ [60]	$dN^{\text{ch}}/d\eta$ [61]
7.7	$dN/dy(\pi^+, K^+, p)$ [55] $\langle p_T \rangle(\pi^+, K^+, p, \bar{p})$ [55] $v_2^{\text{ch}}\{2\}$ [59], $v_3^{\text{ch}}\{2\}$ [60]	

treatment enlarges the model parameter space from 20 to 26 dimensions.

Table II summarizes the experimental observables (604 data points in total) in the current Bayesian inference study. The midrapidity measurements in Au + Au collisions at 200, 19.6, and 7.7 GeV can cover up to $\mu_B \sim 0.4$ GeV in the QCD phase diagram [55–57]. Because the theoretical uncertainty is significant in peripheral collisions, we use identified particle yields and their mean p_T from 0%–5% to 50%–60% centrality and charged hadron $v_n\{2\}$ from central up to 40%–50% centrality. We do not include the antiproton yields at 19.6 and 7.7 GeV because the statistical errors in the training simulations are still too big for reliable model emulation. In our following analysis, we will quantify the impacts of including the pseudorapidity distribution of charged hadron yields and their elliptic flow coefficient from the PHOBOS Collaboration on constraining the QGP properties.

To efficiently explore the parameter space $\{\theta\}$ listed in Table I, we train Gaussian process (GP) emulators for our model calculations with 1000 design points in the model parameter space. These 1000 design points are sampled using the maximum projection latin hypercube design algorithm [63,64]. At every design parameter point, we simulate 1000 minimum bias Au + Au collisions at 200 GeV and 2000 minimum bias events at 19.6 and 7.7 GeV each. An interactive web page with the trained GP emulators is available to help the interested reader develop intuition about how the model parameters affect the observables [65].

Using the trained GP emulators, we can obtain the posterior distribution of model parameters, $\mathcal{P}(\theta|y_{\text{exp}})$, following Bayes' theorem by sampling the uniform prior $\mathcal{P}(\theta)$ with the Monte Carlo Markov chain (MCMC) method, $\mathcal{P}(\theta|y_{\text{exp}}) \propto \mathcal{P}(y_{\text{exp}}|\theta)\mathcal{P}(\theta)$. Here $\mathcal{P}(y_{\text{exp}}|\theta)$ is the likelihood for the model results with parameter θ to agree with the experimental data y_{exp}. It is defined as a multivariate normal distribution [66]. We verify our Bayesian inference analysis with a closure test in the Supplemental Material [67].

Results and discussions.—After performing the Bayesian inference analysis on the STAR and PHOBOS data listed in Table II, we obtain the posterior distribution for our model parameters. In this Letter, we will focus on the constraints on initial-state nuclear stopping and QGP shear and bulk viscosities, which are of primary physics interest. A complete analysis will be reported in the follow-up work.

Figure 1 shows prior and posterior distributions of the average rapidity loss as a function of initial-state rapidity y_{init} in the 3D-Glauber model. The narrowing in the 90% prior for y_{init} between the transition points of the linear parametrization is an artifact of this choice of parametrization. The average rapidity loss is strongly correlated with the amount of particle production in the collisions. The comparison of the 90% prior (the light gray band) with the red band shows that the identified particle yields at the top RHIC energy can constrain the $\langle y_{\text{loss}} \rangle$ for $y_{\text{init}} \in [4, 6]$. This result is consistent with the fact that the incoming
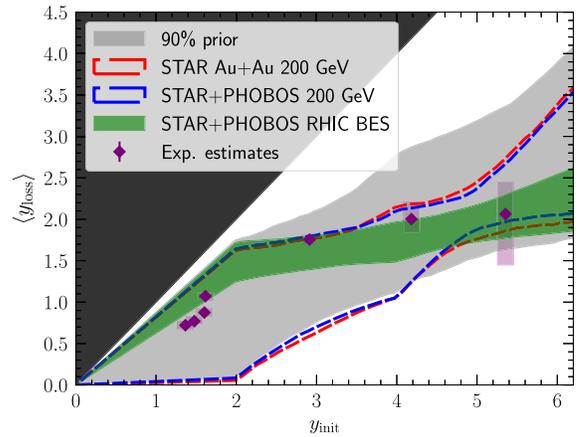
FIG. 1. Posterior distributions of the average initial-state rapidity loss at the nuclear impact. Color bands indicate 90% confidence intervals. The experimental estimate of initial-state nuclear stopping is taken from the net proton rapidity measurements [69,70].
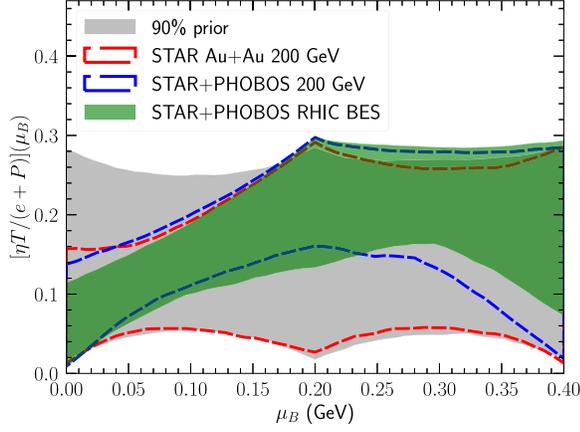
FIG. 2.   Posterior distribution of the μ_B dependent QGP specific shear viscosity. Bands indicate 90% confidence intervals.

nucleons' beam rapidity $y_{\text{beam}} \equiv \text{arccosh}[\sqrt{s_{\text{NN}}}/(2m_{\text{N}})] = 5.36$ at $\sqrt{s_{\text{NN}}} = 200$ GeV [68].

Our analysis suggests that the average rapidity loss at $\sqrt{s_{\text{NN}}} = 200$ GeV is $\langle y_{\text{loss}} \rangle \sim 2$, which is consistent with estimations based on BRAHMS measurements [70]. The mild difference between the red and blue bands in Fig. 1 indicates that the PHOBOS $dN^{\text{ch}}/d\eta$ measurements do not impose any significant additional constraints on the $\langle y_{\text{loss}} \rangle$ parameter, because the data have relatively large error bars compared to the STAR measurements at midrapidity.

Employing the RHIC BES data in the Bayesian analysis results in the green band, which is significantly narrower than the others. This result demonstrates that particle yield measurements from 7.7 to 200 GeV can impose strong constraints on the average rapidity loss for $y_{\text{init}} \leq 6$. Our constraints also agree well with independent experimental estimates from baryon stopping measurements [69,70]. For low energy collisions with $y_{\text{init}} < 2$, our current constraint is slightly larger than the experimental estimates from the E917 and E802/E866 experiments [69]. Future calibrations including these measurements will further refine the rapidity loss constraints at small y_{init}.

Figure 2 shows the posterior distribution for the effective QGP specific shear viscosity as a function of the net baryon chemical potential μ_B. Using only the STAR midrapidity measurements at $\sqrt{s_{\text{NN}}} = 200$ GeV in the Bayesian analysis constrains the effective QGP $\tilde{\eta} = \eta T/(e + P)$ around $\mu_B = 0$. The obtained 90% posterior region is consistent with previous Bayesian analyses assuming longitudinal boost invariance [32,34,35,37–39,41,42]. Notably, including PHOBOS pseudorapidity-dependent observables can significantly improve the constraints on the QGP shear viscosity up to $\mu_B \sim 0.2$ GeV. The sensitivity to $\eta T/(e + P)$ at finite μ_B comes from the fact that the fireballs in the forward and backward rapidity regions probe larger net baryon densities. Therefore, we emphasize that rapidity-dependent measurements at RHIC [61,62] are extremely valuable to
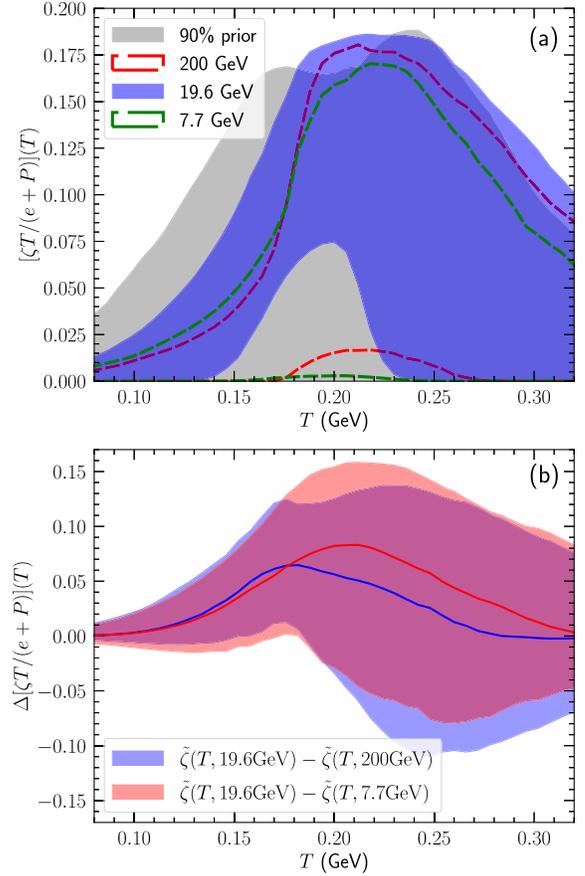
FIG. 3.   Panel (a): Posterior distributions of the temperature dependence of the QGP $\tilde{\zeta}(T) = [\zeta T/(e + P)](T)$ at different collision energies. Panel (b): Posterior distribution of the difference in $[\zeta T/(e + P)](T)$ at 19.6 GeV from the other two collision energies. Solid lines are the median of the $\Delta\tilde{\zeta}(T)$ distributions. Bands indicate 90% confidence levels.

extract the μ_B dependence of the QGP properties. They have further been used to constrain the T dependence of the shear viscosity in the low-temperature regime [71], which in our framework is covered by the URQMD simulations.

Finally, the Bayesian analysis including observables from the full RHIC BES program provides a significant constraint on the QGP $[\eta T/(e + P)](\mu_B)$ up to $\mu_B \sim 0.4$ GeV. We find that the RHIC BES measurements favor the QGP specific shear viscosity to *increase* with μ_B. This conclusion is consistent with previous phenomenological studies [25,30,33] and calculations [72–74], but different from theoretical work in [75,76]. Future studies including a more general $(T - \mu_B)$ dependence of the shear viscosity will result in more robust constraints.

Figure 3(a) shows the posterior constraints on the QGP specific bulk viscosity $\tilde{\zeta}(T) \equiv [\zeta T/(e + P)](T)$. The Bayesian analysis with only the measurements at 200 GeV favors a bulk viscosity peaking around $T = 200$–220 MeV. The constraints at high temperature are relatively weak compared with the 90% prior. The

preferred values of $\tilde{\zeta}(T)$ at $\sqrt{s_{NN}} = 19.6$ GeV are larger than those at 200 and 7.7 GeV for temperatures between 0.15 and 0.2 GeV. This nonmonotonic behavior is further investigated in Fig. 3(b), where we compute the difference $\Delta\tilde{\zeta}(T)$ between 19.6 GeV and the two other collision energies sample-by-sample drawn from the posterior. This treatment ensures that the 90% confidence bands include the correlated variations of $\tilde{\zeta}(T)$ in different posterior samples.

We find a bias of $\Delta\tilde{\zeta}(T)$ towards positive values for temperatures $T \in [0.15, 0.2]$ GeV. Although the 90% confidence bands cover $\Delta\tilde{\zeta}(T) = 0$, our result suggests a nonmonotonic dependence of the QGP bulk viscosity along the net baryon chemical potential direction. Physically, this result could also emerge if there is a softening (and/or hardening) of the equation of state relative to the lattice-QCD-based NEOS-BQS around $\mu_B \sim 0.2(0.4)$ GeV. Our result is consistent with the theory expectation from the STAR two-pion interferometry analyses (often referred to as HBT radii) [77,78]. Therefore, it is essential to include the HBT radii measurements in future Bayesian inference analyses [31] to further improve the statistical significance of this result.

Conclusions.—This work presented the first extraction of temperature and baryon chemical potential dependent QGP transport coefficients from a multisystem Bayesian inference study of particle production, mean transverse momentum, and flow anisotropy in the RHIC BES program using an event-by-event $(3 + 1)$D dynamical framework. Such a study requires large-scale computations, which only became possible recently with significant improvements in the numerical performance of the theoretical framework.

Using measurements from multiple collision energies, we obtained statistically robust constraints on initial-state nuclear stopping, μ_B-dependent QGP shear viscosity, and the QGP bulk viscosity, including its effective μ_B dependence via its variation at different collision energies. Constraints on the average rapidity loss in the initial state are essential to quantitatively understand the longitudinal dynamics in these collisions, such as baryon and charge stopping and longitudinal flow decorrelation. The RHIC BES measurements favor a larger effective QGP specific shear viscosity at finite μ_B than at $\mu_B = 0$. This finding provides valuable insight when confronted with theoretical studies, which differ even qualitatively in the μ_B dependence of $\eta T/(e + P)$ [72,73,75,76].

We find a hint of nonmonotonic dependence of the QGP specific bulk viscosity $\zeta T/(e + P)$ as a function of the collision energy. Because the bulk viscosity decelerates the local expansion, our finding could also indicate a softening of the equation of state for $\mu_B \sim 0.2$ GeV, and/or a hardening at $\mu_B \sim 0.4$ GeV, relative to the employed EOS. For a more conclusive result, a flexible equation of state with variable μ_B dependence should be included in the analysis.

Further, the posterior constraint can be improved by introducing more experimental observables in the future.

Overall, our work marks a significant advancement in extracting QGP properties at finite net baryon density, using systematic global analyses with RHIC BES measurements. It paves the way to phenomenologically quantify the QCD phase diagram and search for a possible critical point and the associated first-order phase transition at large net baryon densities. It will be exciting to confront this theoretical framework with the upcoming RHIC BES phase II measurements and those from the future Facility for Antiproton and Ion Research (FAIR) in Europe.

[1] P. Achenbach *et al.*, The present and future of QCD, arXiv:2303.02579.

[2] M. Arslandok *et al.*, Hot QCD white paper, arXiv:2303.17254.

[3] Helen Caines (STAR Collaboration), The RHIC beam energy scan: STAR's perspective, in *44th Rencontres de Moriond on QCD and High Energy Interactions* (2009), pp. 375–378, arXiv:0906.0305.

[4] Bedangadas Mohanty (STAR Collaboration), STAR experiment results from the beam energy scan program at RHIC, J. Phys. G **38**, 124023 (2011).

[5] Jeffery T. Mitchell (PHENIX Collaboration), The RHIC beam energy scan program: Results from the PHENIX experiment, Nucl. Phys. **A904-905**, 903c (2013).

[6] Grazyna Odyniec, Future of the beam energy scan program at RHIC, EPJ Web Conf. **95**, 03027 (2015).

[7] M. M. Aggarwal *et al.* (STAR Collaboration), An experimental exploration of the QCD phase diagram: The search for the critical point and the onset of de-confinement, arXiv:1007.2613.

[8] Xiaofeng Luo and Nu Xu, Search for the QCD critical point with fluctuations of conserved quantities in relativistic heavy-ion collisions at RHIC: An overview, Nucl. Sci. Tech. **28**, 112 (2017).

[9] Adam Bzdak, Shinichi Esumi, Volker Koch, Jinfeng Liao, Mikhail Stephanov, and Nu Xu, Mapping the phases of

quantum chromodynamics with beam energy scan, Phys. Rep. **853**, 1 (2020).

[10] Xin An *et al.*, The BEST framework for the search for the QCD critical point and the chiral magnetic effect, Nucl. Phys. **A1017**, 122343 (2022).

[11] Chun Shen, Zhi Qiu, Huichao Song, Jonah Bernhard, Steffen Bass, and Ulrich Heinz, The iEBE-VISHNU code package for relativistic heavy-ion collisions, Comput. Phys. Commun. **199**, 61 (2016).

[12] J. H. Putschke *et al.*, The JETSCAPE framework, arXiv: 1903.07706.

[13] Bjoern Schenke, Chun Shen, and Prithwish Tribedy, Running the gamut of high energy nuclear collisions, Phys. Rev. C **102**, 044905 (2020).

[14] Govert Nijs, Wilke van der Schee, Umut Gürsoy, and Raimond Snellings, Bayesian analysis of heavy ion collisions with the heavy ion computational framework Trajectum, Phys. Rev. C **103**, 054909 (2021).

[15] Long-Gang Pang, Hannah Petersen, and Xin-Nian Wang, Pseudorapidity distribution and decorrelation of anisotropic flow within the open-computing-language implementation CLVisc hydrodynamics, Phys. Rev. C **97**, 064918 (2018).

[16] Huichao Song, Steffen A. Bass, Ulrich Heinz, Tetsufumi Hirano, and Chun Shen, 200 A GeV $Au + Au$ collisions serve a nearly perfect quark-gluon liquid, Phys. Rev. Lett. **106**, 192301 (2011); **109**, 139904(E) (2012).

[17] Bjorn Schenke, Sangyong Jeon, and Charles Gale, Elliptic and triangular flow in event-by-event $(3 + 1)D$ viscous hydrodynamics, Phys. Rev. Lett. **106**, 042301 (2011).

[18] Zhi Qiu, Chun Shen, and Ulrich Heinz, Hydrodynamic elliptic and triangular flow in Pb-Pb collisions at $\sqrt{s} = 2.76$ ATeV, Phys. Lett. B **707**, 151 (2012).

[19] Charles Gale, Sangyong Jeon, and Bjoern Schenke, Hydrodynamic modeling of heavy-ion collisions, Int. J. Mod. Phys. A **28**, 1340011 (2013).

[20] Ulrich Heinz and Raimond Snellings, Collective flow and viscosity in relativistic heavy-ion collisions, Annu. Rev. Nucl. Part. Sci. **63**, 123 (2013).

[21] Bjoern Schenke, Chun Shen, and Prithwish Tribedy, Hybrid color glass condensate and hydrodynamic description of the relativistic heavy ion collider small system scan, Phys. Lett. B **803**, 135322 (2020).

[22] Chun Shen and Li Yan, Recent development of hydrodynamic modeling in heavy-ion collisions, Nucl. Sci. Tech. **31**, 122 (2020).

[23] Luis Altenkort, Alexander M. Eller, Anthony Francis, Olaf Kaczmarek, Lukas Mazur, Guy D. Moore, and Hai-Tao Shu, Viscosity of pure-glue QCD from the lattice, Phys. Rev. D **108**, 014503 (2023).

[24] S. Ryu, J. F. Paquet, C. Shen, G. S. Denicol, B. Schenke, S. Jeon, and C. Gale, Importance of the bulk viscosity of QCD in ultrarelativistic heavy-ion collisions, Phys. Rev. Lett. **115**, 132301 (2015).

[25] Iu. A. Karpenko, P. Huovinen, H. Petersen, and M. Bleicher, Estimation of the shear viscosity at finite net-baryon density from $A + A$ collision data at $\sqrt{s_{NN}} = 7.7$–200 GeV, Phys. Rev. C **91**, 064901 (2015).

[26] Chun Shen and Ulrich Heinz, The road to precision: Extraction of the specific shear viscosity of the quark-gluon plasma, Nucl. Phys. News **25**, 6 (2015).

[27] Sangwook Ryu, Jean-François Paquet, Chun Shen, Gabriel Denicol, Björn Schenke, Sangyong Jeon, and Charles Gale, Effects of bulk viscosity and hadronic rescattering in heavy ion collisions at energies available at the BNL relativistic heavy ion collider and at the CERN large hadron collider, Phys. Rev. C **97**, 034910 (2018).

[28] Björn Schenke, Chun Shen, and Prithwish Tribedy, Multiparticle and charge-dependent azimuthal correlations in heavy-ion collisions at the relativistic heavy-ion collider, Phys. Rev. C **99**, 044908 (2019).

[29] H. Niemi, K. J. Eskola, and R. Paatelainen, Event-by-event fluctuations in a perturbative QCD + saturation + hydrodynamics model: Determining QCD matter shear viscosity in ultrarelativistic heavy-ion collisions, Phys. Rev. C **93**, 024907 (2016).

[30] Chun Shen and Sahr Alzhrani, Collision-geometry-based 3D initial condition for relativistic heavy-ion collisions, Phys. Rev. C **102**, 014909 (2020).

[31] Scott Pratt, Evan Sangaline, Paul Sorensen, and Hui Wang, Constraining the equation of state of super-hadronic matter from heavy-ion collisions, Phys. Rev. Lett. **114**, 202301 (2015).

[32] J. E. Bernhard, J. S. Moreland, S. A. Bass, Jia Liu, and Ulrich Heinz, Applying Bayesian parameter estimation to relativistic heavy-ion collisions: Simultaneous characterization of the initial state and quark-gluon plasma medium, Phys. Rev. C **94**, 024907 (2016).

[33] Jussi Auvinen, Jonah E. Bernhard, Steffen A. Bass, and Iurii Karpenko, Investigating the collision energy dependence of η/s in the beam energy scan at the BNL relativistic heavy ion collider using Bayesian statistics, Phys. Rev. C **97**, 044905 (2018).

[34] Jonah E. Bernhard, J. Scott Moreland, and Steffen A. Bass, Bayesian estimation of the specific shear and bulk viscosity of quark-gluon plasma, Nat. Phys. **15**, 1113 (2019).

[35] Govert Nijs, Wilke van der Schee, Umut Gürsoy, and Raimond Snellings, Transverse momentum differential global analysis of heavy-ion collisions, Phys. Rev. Lett. **126**, 202301 (2021).

[36] D. Everett, W. Ke, J. F. Paquet, G. Vujanovic, S. A. Bass *et al.* (JETSCAPE Collaboration), Phenomenological constraints on the transport properties of QCD matter with data-driven model averaging, Phys. Rev. Lett. **126**, 242301 (2021).

[37] D. Everett, W. Ke, J. F. Paquet, G. Vujanovic, S. A. Bass *et al.* (JETSCAPE Collaboration), Multisystem Bayesian constraints on the transport coefficients of QCD matter, Phys. Rev. C **103**, 054904 (2021).

[38] J. E. Parkkila, A. Onnerstad, S. F. Taghavi, C. Mordasini, A. Bilandzic, M. Virta, and D. J. Kim, New constraints for QCD matter from improved Bayesian parameter estimation in heavy-ion collisions at LHC, Phys. Lett. B **835**, 137485 (2022).

[39] J. E. Parkkila, A. Onnerstad, and D. J. Kim, Bayesian estimation of the specific shear and bulk viscosity of the quark-gluon plasma with additional flow harmonic observables, Phys. Rev. C **104**, 054904 (2021).

[40] D. R. Phillips *et al.*, Get on the BAND wagon: A Bayesian framework for quantifying model uncertainties in nuclear dynamics, J. Phys. G **48**, 072001 (2021).

[41] Matthew R. Heffernan, Charles Gale, Sangyong Jeon, and Jean-François Paquet, Early-times Yang-Mills dynamics and the characterization of strongly interacting matter with statistical learning, arXiv:2306.09619.

[42] Matthew R. Heffernan, Charles Gale, Sangyong Jeon, and Jean-François Paquet, Bayesian quantification of strongly-interacting matter with color glass condensate initial conditions, arXiv:2302.09478.

[43] Chun Shen and Björn Schenke, Dynamical initial state model for relativistic heavy-ion collisions, Phys. Rev. C **97**, 024907 (2018).

[44] Chun Shen and Björn Schenke, Longitudinal dynamics and particle production in relativistic nuclear collisions, Phys. Rev. C **105**, 064905 (2022).

[45] Wenbin Zhao, Sangwook Ryu, Chun Shen, and Björn Schenke, 3D structure of anisotropic flow in small collision systems at energies available at the BNL relativistic heavy ion collider, Phys. Rev. C **107**, 014904 (2023).

[46] Akihiko Monnai, Björn Schenke, and Chun Shen, Equation of state at finite densities for QCD matter in nuclear collisions, Phys. Rev. C **100**, 024907 (2019).

[47] Bjoern Schenke, Sangyong Jeon, and Charles Gale, $(3 + 1)$D hydrodynamic simulation of relativistic heavy-ion collisions, Phys. Rev. C **82**, 014903 (2010).

[48] Jean-François Paquet, Chun Shen, Gabriel S. Denicol, Matthew Luzum, Björn Schenke, Sangyong Jeon, and Charles Gale, Production of photons in relativistic heavy-ion collisions, Phys. Rev. C **93**, 044906 (2016).

[49] Gabriel S. Denicol, Charles Gale, Sangyong Jeon, Akihiko Monnai, Björn Schenke, and Chun Shen, Net baryon diffusion in fluid dynamic simulations of relativistic heavy-ion collisions, Phys. Rev. C **98**, 034916 (2018).

[50] A. Bazavov et al. (HotQCD Collaboration), Chiral crossover in QCD at zero and non-zero chemical potentials, Phys. Lett. B **795**, 15 (2019).

[51] Szabolcs Borsanyi, Zoltan Fodor, Jana N. Guenther, Ruben Kara, Sandor D. Katz, Paolo Parotto, Attila Pasztor, Claudia Ratti, and Kalman K. Szabo, QCD crossover at finite chemical potential from lattice simulations, Phys. Rev. Lett. **125**, 052001 (2020).

[52] S. A. Bass et al., Microscopic models for ultrarelativistic heavy ion collisions, Prog. Part. Nucl. Phys. **41**, 255 (1998).

[53] M. Bleicher et al., Relativistic hadron hadron collisions in the ultrarelativistic quantum molecular dynamics model, J. Phys. G **25**, 1859 (1999).

[54] M. Teslyk, L. Bravina, O. Panova, O. Vitiuk, and E. Zabrodin, Shear viscosity in microscopic calculations of $A + A$ collisions at energies available at the Nuclotron-based Ion Collider fAcility (NICA), Phys. Rev. C **101**, 014904 (2020).

[55] L. Adamczyk et al. (STAR Collaboration), Bulk properties of the medium produced in relativistic heavy-ion collisions from the beam energy scan program, Phys. Rev. C **96**, 044904 (2017).

[56] J. Cleymans, H. Oeschler, K. Redlich, and S. Wheaton, Comparison of chemical freeze-out criteria in heavy-ion collisions, Phys. Rev. C **73**, 034905 (2006).

[57] A. Andronic, P. Braun-Munzinger, and J. Stachel, The Horn, the hadron mass spectrum and the QCD phase diagram: The Statistical model of hadron production in central nucleus-nucleus collisions, Nucl. Phys. **A834**, 237C (2010).

[58] B. I. Abelev et al. (STAR Collaboration), Systematic measurements of identified particle spectra in pp, d^+ Au and Au + Au collisions from STAR, Phys. Rev. C **79**, 034909 (2009).

[59] L. Adamczyk et al. (STAR Collaboration), Harmonic decomposition of three-particle azimuthal correlations at energies available at the BNL relativistic heavy ion collider, Phys. Rev. C **98**, 034918 (2018).

[60] L. Adamczyk et al. (STAR Collaboration), Beam energy dependence of the third harmonic of azimuthal correlations in Au + Au collisions at RHIC, Phys. Rev. Lett. **116**, 112302 (2016).

[61] B. B. Back et al. (PHOBOS Collaboration), Charged-particle pseudorapidity distributions in Au + Au collisions at $s(NN)^{1/2} = 62.4$ GeV, Phys. Rev. C **74**, 021901 (2006).

[62] B. Alver et al. (PHOBOS Collaboration), System size, energy, pseudorapidity, and centrality dependence of elliptic flow, Phys. Rev. Lett. **98**, 242302 (2007).

[63] Evren Gul V. Roshan Joseph and Shan Ba, Designing computer experiments with multiple types of factors: The maxpro approach, J. Quality Technol. **52**, 343 (2020).

[64] V. Roshan Joseph, Evren Gul, and Shan Ba, Maximum projection designs for computer experiments, Biometrika **102**, 371 (2015).

[65] The interactive web page is powered by Streamlit, https://3dglauberappapp-bbbfxt8w75lbvnkcxreahl.streamlit.app.

[66] Heikki Mäntysaari, Björn Schenke, Chun Shen, and Wenbin Zhao, Bayesian inference of the fluctuating proton shape, Phys. Lett. B **833**, 137348 (2022).

[67] See Supplemental Material at http://link.aps.org/supplemental/10.1103/PhysRevLett.132.072301 for a closure test for the Bayesian inference for initial-state rapidity loss and QGP shear and bulk viscosities at the RHIC Beam Energy Scan program.

[68] Chun Shen and Björn Schenke, Dynamical initialization and hydrodynamic modeling of relativistic heavy-ion collisions, Nucl. Phys. **A982**, 411 (2019).

[69] F. Videbæk and Ole Hansen, Baryon rapidity loss and midrapidity stacking in high energy nucleus-nucleus collisions, Phys. Rev. C **52**, 2684 (1995).

[70] I. C. Arsene et al. (BRAHMS Collaboration), Nuclear stopping and rapidity loss in Au + Au collisions at s(NN) ∗ ∗(1/2) = 62.4-GeV, Phys. Lett. B **677**, 267 (2009).

[71] Gabriel Denicol, Akihiko Monnai, and Bjoern Schenke, Moving forward to constrain the shear viscosity of QCD matter, Phys. Rev. Lett. **116**, 212301 (2016).

[72] C. Hoyos, M. Jarvinen, N. Jokela, J. G. Subils, J. Tarrio, and A. Vuorinen, Transport in strongly coupled quark matter, Phys. Rev. Lett. **125**, 241601 (2020).

[73] Olga Soloveva, David Fuseau, Jörg Aichelin, and Elena Bratkovskaya, Shear viscosity and electric conductivity of a hot and dense QGP with a chiral phase transition, Phys. Rev. C **103**, 054901 (2021).

[74] Emma McLaughlin, Jacob Rose, Travis Dore, Paolo Parotto, Claudia Ratti, and Jacquelyn Noronha-Hostler, Building a testable shear viscosity across the QCD phase diagram, Phys. Rev. C **105**, 024903 (2022).

[75] Gabriel S. Denicol, Charles Gale, Sangyong Jeon, and Jorge Noronha, Fluid behavior of a baryon-rich hadron resonance gas, Phys. Rev. C **88**, 064901 (2013).

[76] J. Grefa, M. Hippert, J. Noronha, J. Noronha-Hostler, I. Portillo, C. Ratti, and R. Rougemont, Transport coefficients of the quark-gluon plasma at the critical point and across the first-order line, Phys. Rev. D **106**, 034024 (2022).

[77] L. Adamczyk *et al.* (STAR Collaboration), Beam-energy-dependent two-pion interferometry and the freeze-out eccentricity of pions measured in heavy ion collisions at the STAR detector, Phys. Rev. C **92**, 014904 (2015).

[78] Roy A. Lacey, Indications for a critical end point in the phase diagram for hot and dense nuclear matter, Phys. Rev. Lett. **114**, 142301 (2015).

[79] Ruth Pordes *et al.*, The open science grid, J. Phys. Conf. Ser. **78**, 012057 (2007).

[80] Igor Sfiligoi, Daniel C. Bradley, Burt Holzman, Parag Mhashilkar, Sanjay Padhi, and Frank Wurthwrin, The pilot way to grid resources using glideinWMS, WRI World Congr. **2**, 428 (2009).